

# Modeling ion extraction from a free-plasma surface with a flexible conformal mesh

**STANLEY HUMPHRIES JR.**

*Field Precision, PO Box 13595,  
Albuquerque, New Mexico 87192*

## **Abstract**

This paper describes a new method for numerical modeling of extraction of high-current ion beams from a plasma source. The challenge in the application is to satisfy simultaneously requirements for space-charge-limited flow and uniform ion flux. The plasma surface must assume a special shape that is not known in advance. The method involves the use of finite-element techniques coupled with a dynamic conformal mesh. Starting from an initial estimate, the flexible mesh is shifted to achieve uniform flux over the emission surface. The approach achieves high accuracy and has the versatility to handle complex emission surfaces in gridded guns. The technique can also be applied to determine cathode shapes for uniform-flux electron guns. Benchmark calculations using the Trak two-dimensional ray-tracing code are described. The program automatically carries out the surface search.

# Modeling ion extraction from a free-plasma surface with a flexible conformal mesh

STANLEY HUMPHRIES JR.

*Field Precision, PO Box 13595,  
Albuquerque, New Mexico 87192*

## 1. Introduction

Ray-tracing codes [1-6] are standard tools for the design of steady-state, high-current electron guns. The programs represent a beam by a finite number  $N_p$  of model particles. The particles follow the trajectories of individual electrons but carry a fraction  $\sim 1/N_p$  of the beam charge and current. The first stage in the iterative procedure is to calculate applied electric and magnetic fields and to trace the model-particle orbits, assigning beam charge and current to the mesh. The fields are updated to reflect the beam contributions, and then orbits are recalculated. With several iteration cycles and proper averaging, the fields and orbits converge to a self-consistent solution.

The design of ion guns with plasma sources poses an additional challenge. While the source shape for electron extraction from a thermionic cathode is specified, the surface for ion extraction from a freely-expanding plasma is not known in advance. The surface position is determined by the balance between incoming ion flux and space-charge-limited current density. For a given extractor geometry, there is a unique surface shape that simultaneously satisfies the Child law and ensures that the space-charge-limited current density is uniform.

Existing computer codes [7-11] for ion-beam generation apply finite-difference techniques on static box meshes. This paper describes a new approach that uses finite-element techniques with a dynamic conformal mesh. Here the mesh flexes in response to the local space-charge-limited current density, adjusting to a shape that guarantees uniform extracted ion flux. The method preserves the accuracy advantage of conformal meshes for field calculations near slanted or curved surfaces. Furthermore, the versatile conformal mesh approach is not limited to simple curves and can be applied to gridded guns. The method is also useful for electron gun calculations where the goal is to determine a surface shape that ensures uniform current density. The following section reviews methods to treat Child-law emission on a conformal mesh and the nature of the plasma source surface (often called the *plasma meniscus*). Section 3 details the steps in the computational procedure while Section 4 summarizes baseline calculations performed with the Trak code [6].

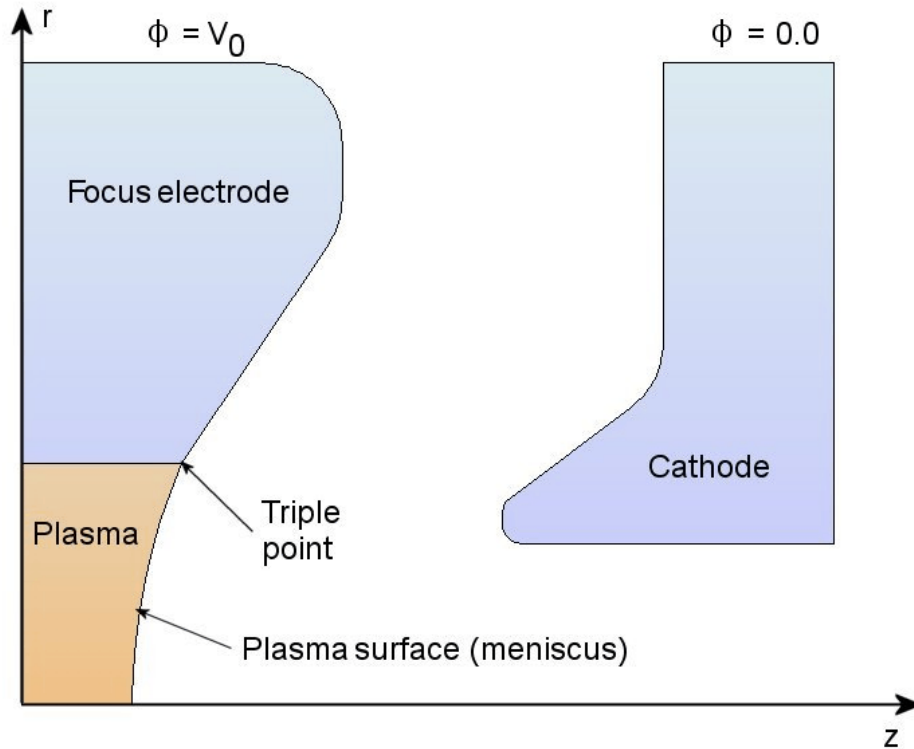


**Figure 1.** Terminology for and schematic geometry of an ion gun with a plasma source.

## 2. Space-charge limited ion emission from a plasma surface

This section briefly reviews the numerical calculation of space-charge-limited flow and the nature of the plasma source surface. Reference 12 gives a detailed discussion of Child-law emission, the Bohm current density and the formation of a plasma meniscus.

The fundamental difficulty in a numerical calculation of space-charge-limited flow is that the electric field approaches zero on the source surface. Therefore, it is impossible to initiate numerical orbit integrations. The standard solution is to generate particles on a virtual emission surface a short distance  $D_e$  from the source surface. The electric field always has a non-zero value on the emission surface. Model particles are assigned two quantity: 1) a momentum based on the electrostatic potential difference between the source and emission surfaces and 2) a current based on application of the Child law over the thin gap. Reference 13 describes an emission-surface procedure that is well-suited to conformal meshes. The method achieves high accuracy by initially back-projecting particle orbits to assign space-charge in the space between the surfaces. In a Pierce-diode benchmark simulation, the technique demonstrates an absolute accuracy in emitted current better than 0.03%. The technique is applicable to ion extraction for a known plasma surface location.

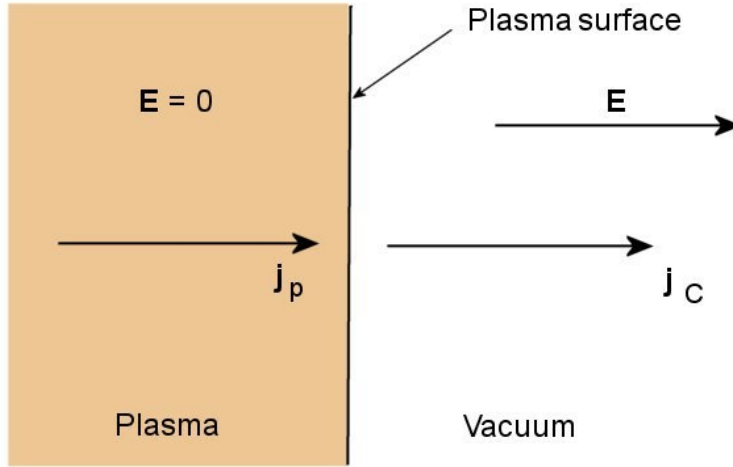


**Figure 2.** Factors that determine the plasma source location, one-dimensional model.

Proceeding to ion extraction, we must first define the term *free plasma surface*. Assume that plasma ions generated by a source expand in a field-free region through an aperture into an acceleration gap with an applied electric field (Fig. 1). The source surface is the transition between the field-free plasma environment and the vacuum flow region. Its location is determined by a balance between the plasma ion flux (which we shall denote by an effective ion current density  $j_p$ ) and the vacuum current density  $j_c$  governed by the Child law. In the one-dimensional geometry shown in Fig. 2, the space-charge-limited current density for ions with charge-state  $Z_i$  and mass  $m_i$  in a gap of width  $d$  and applied voltage  $V_0$  is given by the expression [14]:

$$j_c = \frac{4\epsilon_0}{9} \sqrt{\frac{2Z_i e}{m_i}} \frac{V_0^{3/2}}{d^2} . \quad (1)$$

If the ion flux exceeds the vacuum current limit ( $j_p > j_c$ ), then the plasma expands to reduce the gap width  $d$  until flux balance is achieved:

$$j_p = j_c . \quad (2)$$

In this case, the source surface in Fig. 2 would move to the right. Conversely, if  $j_p < j_c$  the surface recedes to the left. In most plasma sources for ion generation, the ion temperature is much smaller than the electron temperature ( $T_e$ ). In this case, the available effective ion current density is given by the Bohm expression :

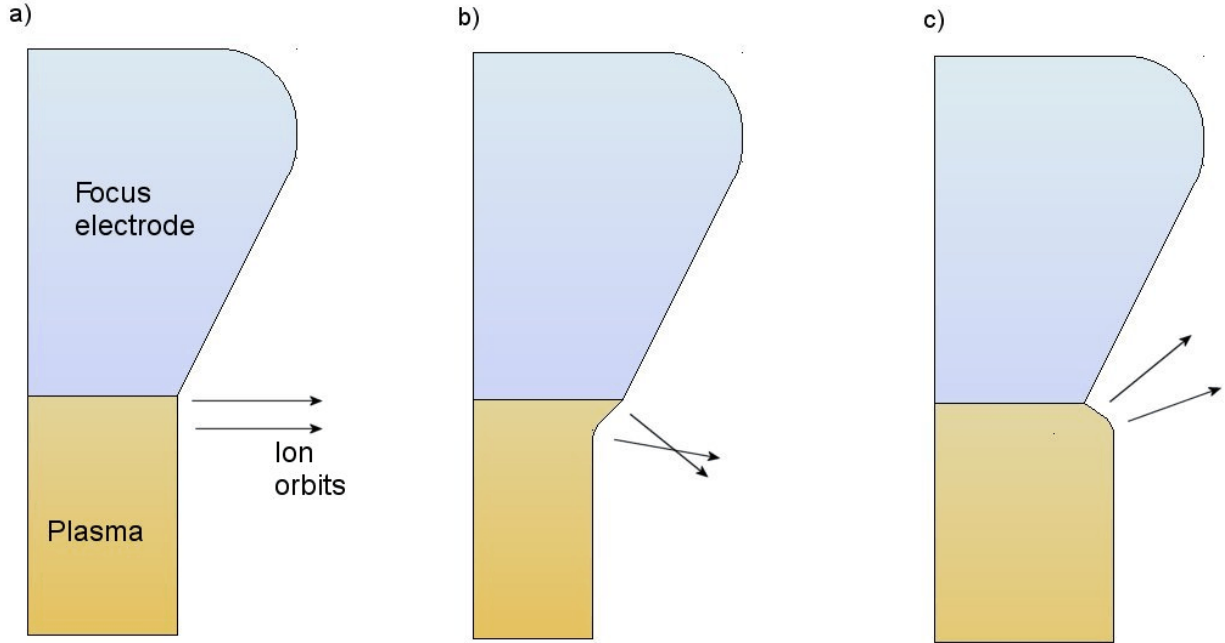


**Figure 3.** Shape of the plasma surface at the triple point and its effect on edge ion orbits. *a)* Balance of plasma ion flux and space-charge-limited current density. *b)* Low plasma flux. *c)* High plasma flux.

$$j_p \cong 0.6 e Z_i n_i \sqrt{kT_e/m_i} . \quad (11.3)$$

We assume a homogenous plasma so that  $j_p$  is uniform over the source surface. This condition sets the primary goal of a plasma extraction calculation: for given applied voltages and surrounding electrode geometries, find a shape of the source surface that guarantees a uniform value of  $j_c$ . A critical concern is the nature of the source surface at the *triple point*: the intersection of the plasma, the aperture electrode and the vacuum acceleration region (Fig. 1). Figure 3a shows the desired condition where the value of  $j_p$  and  $j_c$  at the triple point allow a smooth connection of the source surface to the focus electrode. A reduction in  $j_p$  from this value causes the plasma surface to move into the aperture. If the surface could recede at the triple point, the focus electrode would act as an electrostatic shield giving a large reduction in  $j_c$  at the beam edge. The implication is that the plasma surface is effectively tied to the aperture at the triple point. A low value of  $j_p$  gives a distorted source surface (Fig.3b) with attendant poor extracted beam optics. Conversely, a value of  $j_p$  above the optimum causes the plasma to bulge into the extraction gap giving in a divergent beam (Fig. 3c).

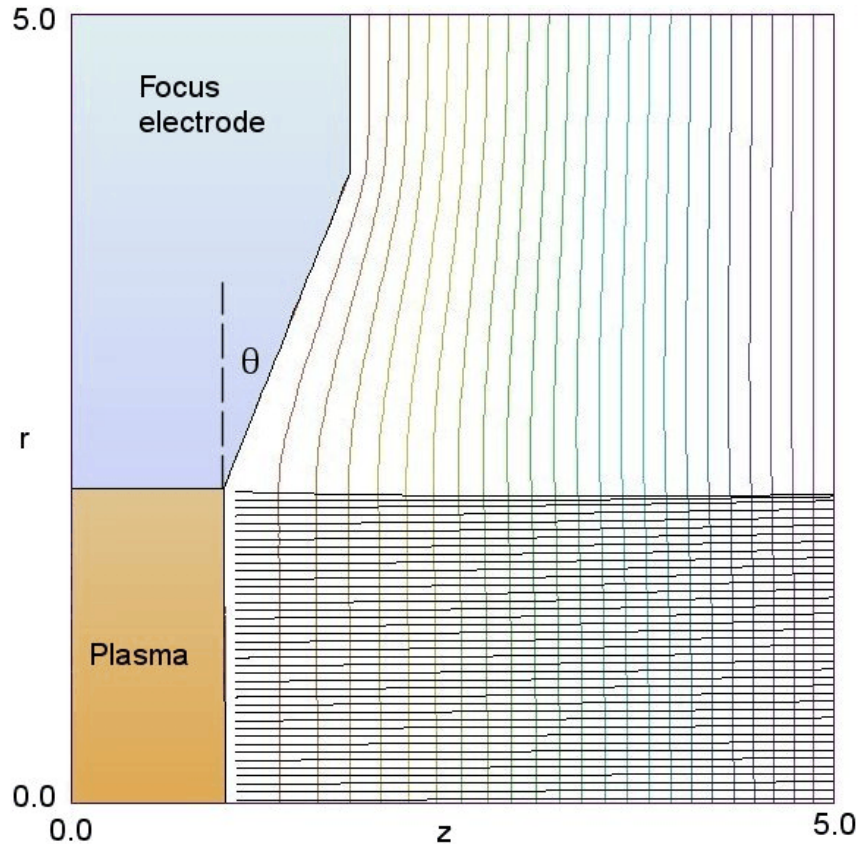


**Figure 4.** Calculation of ion extraction from a plasma surface for an injector with a planar cathode and focus electrode inclined at the Pierce angle,  $\theta = 22.5^\circ$ . (Dimensions in cm.)

In summary, there are two constraints that determine a valid plasma surface solution:

- The value of  $j_c$  must be uniform.
- The plasma surface must connect smoothly to the focus electrode at the triple point.

The combination of the two conditions with specified electrodes and applied voltages defines: 1) a unique plasma surface shape and 2) a required value of the plasma flux  $j_p$ .

Figure 4 illustrates the nature of the plasma meniscus in a two-dimensional extractor. The figure shows an ion gun with a planar cathode and a focus electrode inclined at the angle  $\theta = 22.5^\circ$ . The geometry approximates the ideal Pierce diode [15] with the exception of the cathode shape. Therefore, we expect that the self-consistent plasma surface will approximate a plane connected to the triple point and that the matched plasma flux  $j_p$  will be close to the value predicted by Eq. (1). Suppose we increase the focus-electrode angle (Fig. 5a). The extra metal

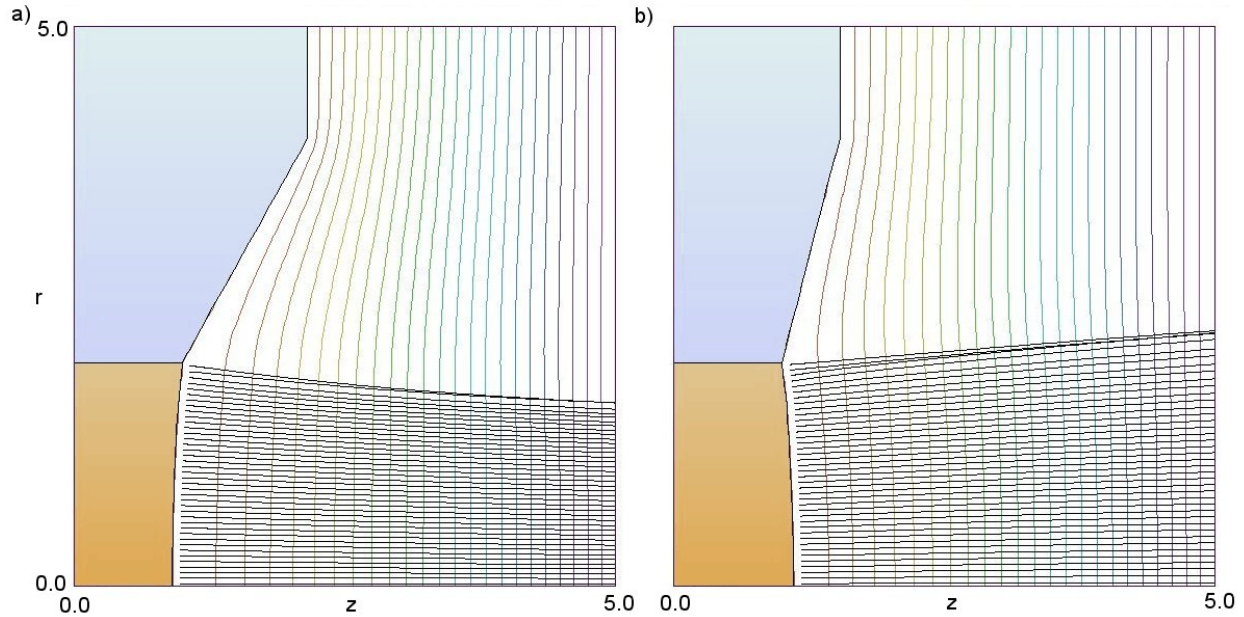


**Figure 5.** Calculations of plasma surface shape and ion extraction for different values of the focus electrode angle. a)  $\theta = 30.0^\circ$ . b)  $\theta = 15.0^\circ$ . (Dimensions in cm)

reduces the electric field on the outer edge of the aperture, suppressing the space-charge-limited current density. Therefore, ion emission would be nonuniform over a flat source surface. To ensure uniform flux the plasma meniscus must assume a concave shape that reduces the current density near the axis. Conversely, a shallow focus-electrode angle ( $\theta < 22.5^\circ$ ) results in enhanced field at the aperture edge. Here the plasma bulges into the acceleration gap to increase current density near the axis (Fig. 5b). The examples suggest a logical procedure for the design of a practical ion gun:

- Starting from the approximate Pierce solution with flat emission surface we add an exit aperture at the cathode. The aperture reduces the electric-field amplitude on the plasma surface near the axis. With no other changes, the plasma would protrude into the acceleration gap.
- We increase the angle of the focus electrode ( $\theta > 22.5^\circ$ ) to suppress emission near the edge, thereby flattening the plasma surface.
- A further increase in the focus electrode angle would give a concave plasma surface and hence a converging beam. In this case, it is possible to use a smaller aperture, reducing the aperture effect on field uniformity over the source surface.
- Additional changes in the shapes of the focus electrode, cathode and (possibly) intermediate electrodes can lead to a beam with the desired characteristics. The solution also constrains the required value of source flux for given applied voltages.

### 3. Computational procedure

The discussion in this section and the examples in the following section are based on Trak [6], a two-dimensional ray-tracing code that employs a structured conformal triangular mesh. The method can be extended to three-dimensional calculations and to other conformal mesh types. The first step in a solution is to generate a mesh that represents the gun geometry. Information must be included that enables the ray-tracing program to identify the following: 1) nodes and element facets of the plasma source surface and 2) surrounding nodes that can be shifted in response to surface flexing. Figure 6 shows features of an input mesh for Trak. It includes a region of non-zero volume to represent the plasma. The region must have enough depth (*i.e.*, number of elements parallel to the flex direction) to accommodate surface displacements. The initial shape of the plasma surface is a guess (usually a flat surface) that connects smoothly at the triple point. Shared nodes along the intersection of the plasma and focus electrode are assigned to the electrode region so that the shape of the metal surface does not change. The mesh is used for a calculation of the initial electric field solution that is passed to the ray-tracing program. In the electrostatic solution both the plasma and the focus electrode are treated as fixed-potential regions with the same applied voltage.

At the beginning of the run Trak inspects the mesh to identify facets and nodes of the source surface (Fig. 6). Source facets lie between an element with the plasma region number and one with the region number of vacuum. The ends of the facets define the flexible plasma surface nodes (with the exception of the node at the triple point). The program orders source facets to form a connected set with respect to distance from the axis for the calculation of the effective area associated with each model particle. The program then determines a set of unit vectors normal to the source facets that point out of the plasma region. The vectors are projected a distance  $D_e$  to define the nodes and facets of the emission surface for the Child-law calculation. Trak then generates one or more model particles per emission facet and performs the standard calculation of space-charge-limited flow using the method of Ref. 13.

After the space-charge solution stabilizes, Trak calculates the current density on the source facets by averaging model particle currents at the emission surface. The current density at the source surface is determined by back-projection with compensation for curvature. The calculated values have small variations on the order of the mesh element size because of systematic errors in the field interpolation. Therefore, it is essential to smooth the spatial variation of current density along the surface to prevent the unstable growth of surface ripples during the adjustment. Trak applies a least-squares-fit to an eighth-order polynomial in  $r$ . Only even terms are included if the plasma surface intersects the axis of symmetry. The fit is weighted by  $r$  for cylindrical solutions. The value of emitted current density at each surface node ( $j_n$ ) is computed by averaging the values on adjacent facets. The program also computes node unit vectors by averaging vectors of adjacent source facets. The position of each node is moved along the corresponding unit vector a distance  $\Delta$  given by:

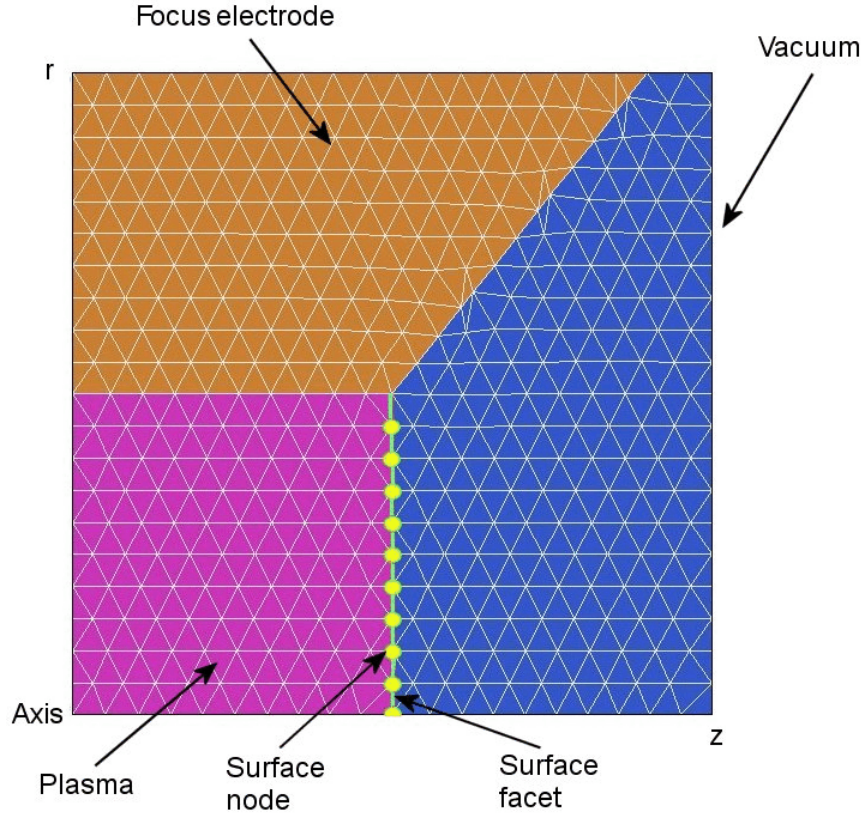


**Figure 6.** Trak structured conformal triangular mesh, showing plasma surface nodes and facets.

$$\Delta = \frac{\alpha d}{2} \left( 1 - \frac{j_n}{j_{out}} \right). \quad (4)$$

Equation (4) follows from the scaling of Eq. (1). The quantity  $d$  is the width of the acceleration gap,  $\alpha$  is a safety factor to ensure stability  $j_{out}$  is the current density on the source facet adjacent to the triple point. Normalizing displacements to  $j_{out}$  ensures that the plasma surface intersects the triple point at a small angle. Note that the direction of the shift in Eq. (4) is away from the acceleration gap (into the plasma) when  $j_n > j_{out}$ . In this case the shift gives a local reduction in the space-charge-limited current density.

After displacement of the source nodes, the positions of neighboring plasma and vacuum nodes must be adjusted to preserve element integrity. Trak employs an iterative mesh relaxation procedure where nodes are shifted toward the average position of the six neighboring nodes. After mesh relaxation, the program checks for inverted elements and makes local corrections to

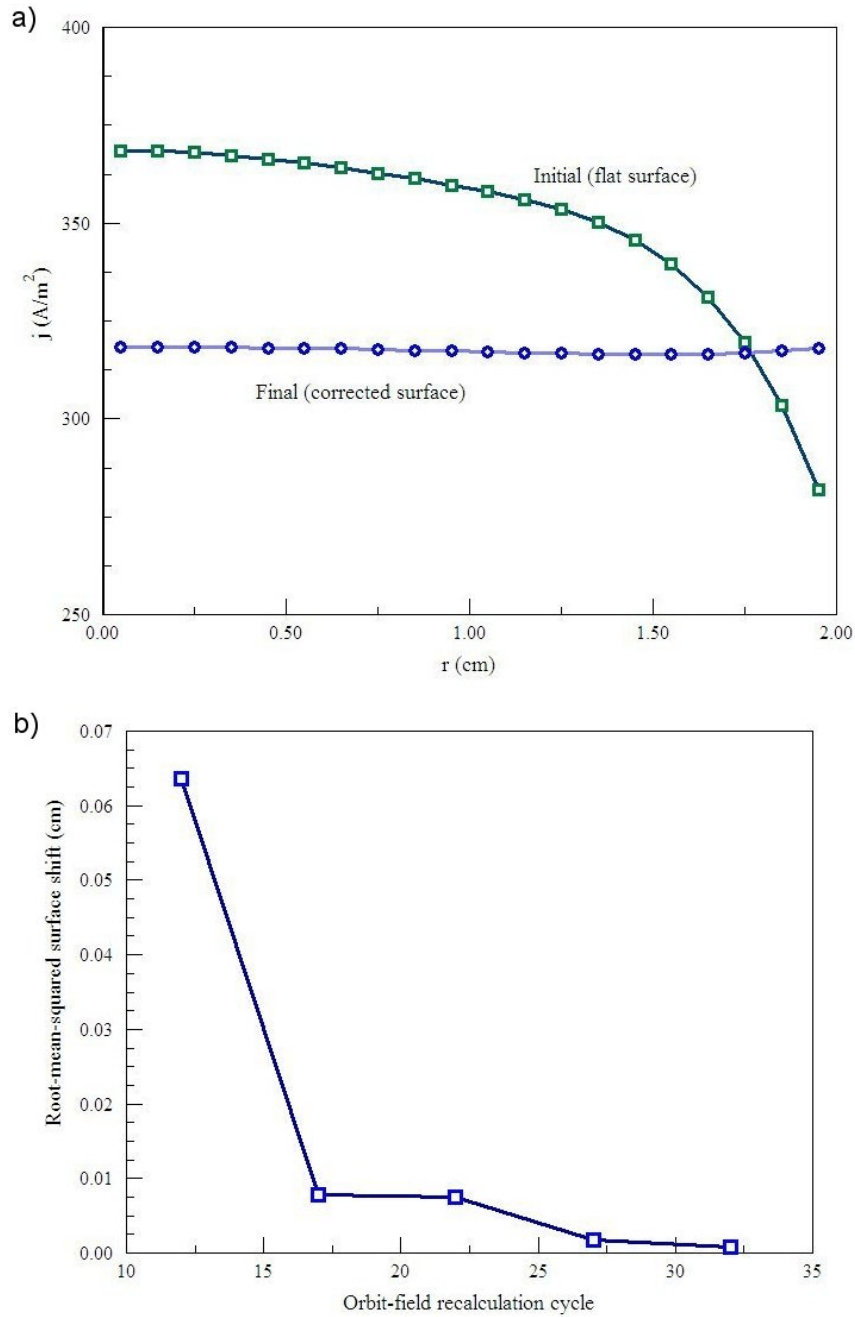


**Figure 7.** Calculation for the geometry of Fig. 5a with 5 surface adjustments. *a*) Radial variation of smoothed current density, initial (flat surface) and final. *b*) Convergence of the calculation, root-mean-squared surface node displacement as a function of orbit-field iteration cycle.

the element nodes. The extensive error checking ensures robust code operation. After surface node shifts and mesh corrections, Trak computes normal vectors for the modified plasma surface and constructs a new emission surface. The program then carries out several standard orbit-field iteration cycles to find a space-charge-limited emission solution for the new source geometry. Trak then uses the stable solution to make further corrections to the source surface according to Eq. (4). A accurate solution typically requires 4-8 surface corrections.

The model has some physical limitations. It does not apply to systems with a strong magnetic field transverse to the extraction direction (*i.e.*, magnetically-insulated ion diodes, transverse extraction from a Penning source,...). In this case, the condition  $j_p = j_C$  may not hold. On the other hand, the procedure can give useful information when the source (such as a duoplasmatron) has sufficient shielding to isolate the magnetic field from the extraction surface. The model also does not hold for sources that produce a mixture of ion species or charge states. In this case the behavior of the extraction sheath is more complex than the simple Child-law description. For example, with multiple charge states the electrostatic sheath may have a complex variation of potential leading to preferential extraction of high-charge-state ions.

## 4. Benchmark calculations

The Trak code was used to calculate the surfaces illustrated in Fig. 4 and 5. The geometry in Fig. 4 is close to an ideal Pierce gun, with the exception that the cathode is a plane rather than a shaped surface that curves away from the anode. The cylindrical injector has an aperture radius of 2.0 cm and gap of width  $d = 4.0$  cm. The simulation used an element width of 0.050 cm near the source and an emission surface spacing of  $D_e = 0.075$  cm. There were 40 source facets and 80 model particles. With four surface adjustments, Trak calculated a current density of 402.6 A/m<sup>2</sup> uniform to within 0.06% over the surface. For comparison, the prediction of Eq. (1) is slightly lower as expected,  $j_C = 380.5$  A/m<sup>2</sup>. The uniform-current-density surface was slightly convex, protruding a distance 0.009 cm at the axis. Similar parameters were used for the examples of Fig. 5a and 5b where the focus electrode angles were  $\theta = 30^\circ$  and  $\theta = 15^\circ$ . For these geometries the current density was nonuniform on the initial flat surface. Figure 7a shows the initial and corrected radial variations of current density for the solution of Fig. 5a. Figure 7b shows the convergence history with the number of orbit-field iteration cycles. The plotted quantity is the root-mean-squared average of source node displacements. Five surface adjustments were performed with five intervening orbit-field iterations to stabilize the space-charge-limited flow solution.

To conclude, we discuss a solution that illustrates a practical application of the technique. We consider a multi-electrode deuteron injector designed at Lawrence Berkeley Laboratory (cited in Ref. 12, p. 326). Figure 8 shows the geometry. The slot injector is part of a vertical array with field symmetry boundaries at the top and bottom and a particle reflection boundary at the bottom. The accel-decel configuration prevents the backflow of electrons from the downstream neutralizing plasma. The region on the right-hand side represents a ground electrode and an assumed profile for the exit plasma. In the first calculation the source plasma surface with 20

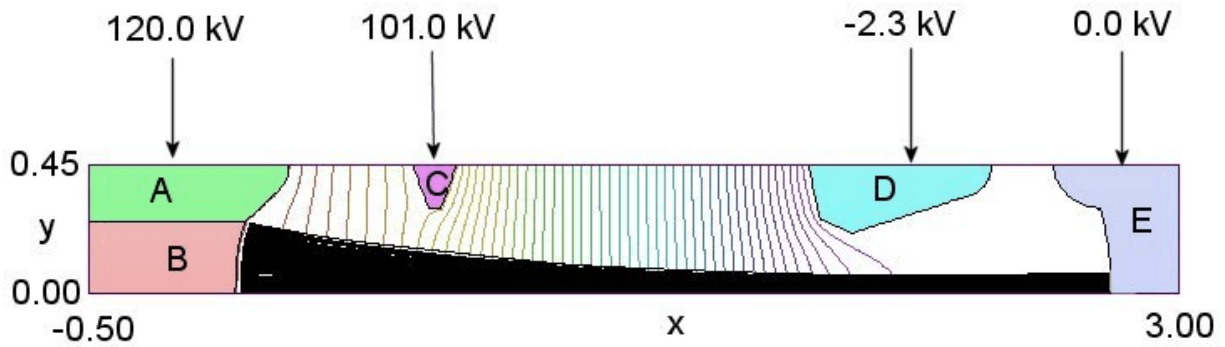


**Figure 8.** Design for a multi-electrode deuteron injector showing one-half of a slot in a vertical array. *A*: focus electrode, *B*: plasma, *C*: extractor electrode, *D*: Decel electrode, *E*: Ground electrode and neutralizing plasma. (Courtesy, W. Cooper, Lawrence Berkeley Laboratory.)

facets was assumed to be initially flat, intersecting the axis at  $z = 0.0$  cm. The mesh contained 7121 variable-potential nodes with an element width  $\sim 0.0125$  cm. The emission surface displacement was  $D_e = 0.0175$  cm. The simulation used 160 model particles with an initial angular spread of  $15^\circ$  at the emission surface. The calculation ran for 72 orbit-field iterations with 8 surface adjustments. The run time was 282 seconds on a 2 GHz computer. The root-mean-squared surface shift was 0.0128 cm on the first displacement and 0.00042 cm on the eighth. In the final state the plasma surface had a concave shape – the surface position on axis was  $z = -0.0315$  cm. Figure 9 shows the initial and final states of the dynamic mesh near the plasma surface. The current density on the initial flat surface varied from 3292 A/m<sup>2</sup> at the center to 1798 A/m<sup>2</sup> at the triple point. In the final state the current density on source facets was  $2494 \pm 22$  A/m<sup>2</sup>, corresponding to a uniformity better than 1 per cent.

To achieve higher accuracy, a second solution was created using the first solution to improve the initial estimate of the plasma surface. The surface was represented as a cylindrical section that crossed the axis at  $z = -0.0315$  cm. After four cycles of surface correction, the code produced the smooth surface shown in Fig. 10 that crossed the axis at  $z = -0.0274$  cm. The current density in the final state was  $2585 \pm 3.4$  A/m<sup>2</sup> with a relative variation between source facets of only 0.13%. In summary, the flexible conformal-mesh technique can generate constant current-density surfaces in planar or cylindrical geometries with high accuracy. In the Trak code, the mesh adjustment operations are performed automatically. The only additional activity on the part of the user beyond setting up a standard space-charge calculation is to supply values for the number of surface adjustments and the number of orbit-field cycles per adjustment.

I am grateful to Schlumberger Princeton Technical Center for their support of this work.

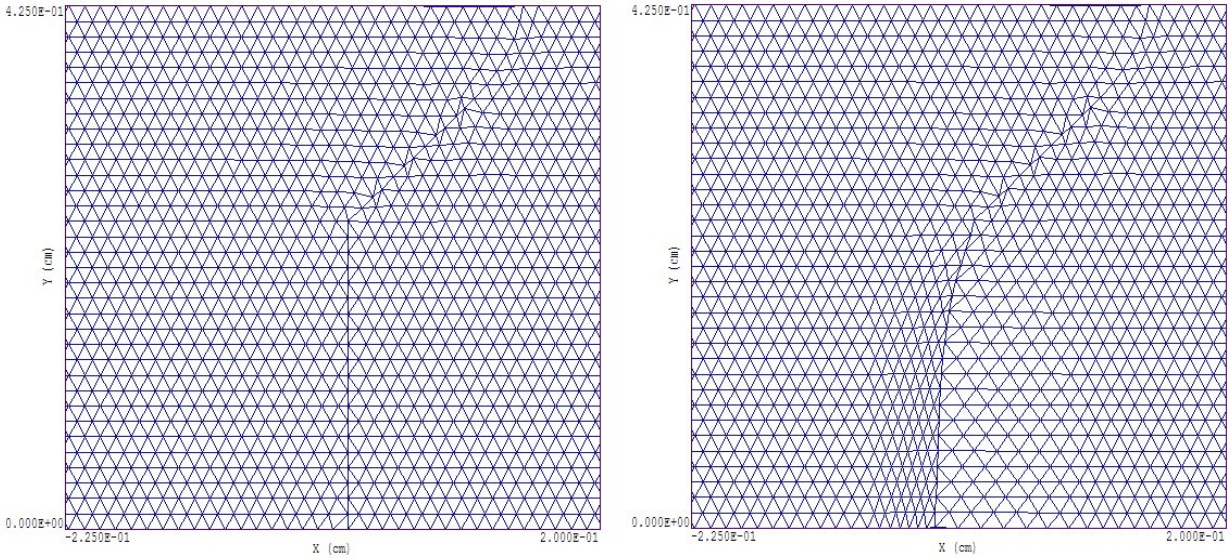


**Figure 9.** Detail of mesh near the plasma surface and triple point, example of Fig. 8. *a)* Initial mesh with assumed flat plasma surface. *b)* Final flexed mesh for uniform current density.

## References

1. W. B. Herrmannsfeldt, Stanford Linear Acc. Center, SLAC-331, 1988 (unpublished).
2. A. C. Paul, Lawrence Berkeley Lab, LBL-13241, 1982 (unpublished).
3. D. L. Vogel, Lawrence Berkeley Lab., LBL-18871, 1985 (unpublished).
4. J. E. Boers, Sandia National Labs, SAND 79-1027, 1980 (unpublished).
5. R. True, IEEE Trans. Nucl. Sci. **NS-32**, 2611 (1985)
6. S. Humphries in **Computational Accelerator Physics**, edited by R. Ryne (Am. Inst. of Phys., New York, 1994), 597 and in **Beams 94: Proceedings, 10th Conf High Power Particle Beams** (National Technical Information Service, NTIS PB95-144317, 1995), 568.
7. J. C. Whitson, J. Smith and J. H. Whealton, J. Comp. Phys. **28** (1978) 408.
8. J. H. Whealton, M. A. Bell, R. J. Raridon, K. E. Rothe and P. M. Ryan, J. App Phys. **64** (1988) 6210.
9. J. E. Boers, IEEE Cat. No. 93CH3334-0 (1993) 213.
10. P. Spadtke, GSI-Report 9 (1983).
11. R. Becker and W. B. Herrmannsfeldt, Rev. Sci. Instrum. **63** (1992) 2756.
12. S. Humphries, **Charged Particle Beams** (Wiley, New York, 1990), Chap. 6 and 7.
13. S. Humphries, J. Computational Phys. **125**, 448 (1996).
14. C. D. Child, Phys. Rev. **32**, 492 (1911).
15. J.R. Pierce, **Theory and Design of Electron Beams** (Van Nostrand, Princeton, 1949).

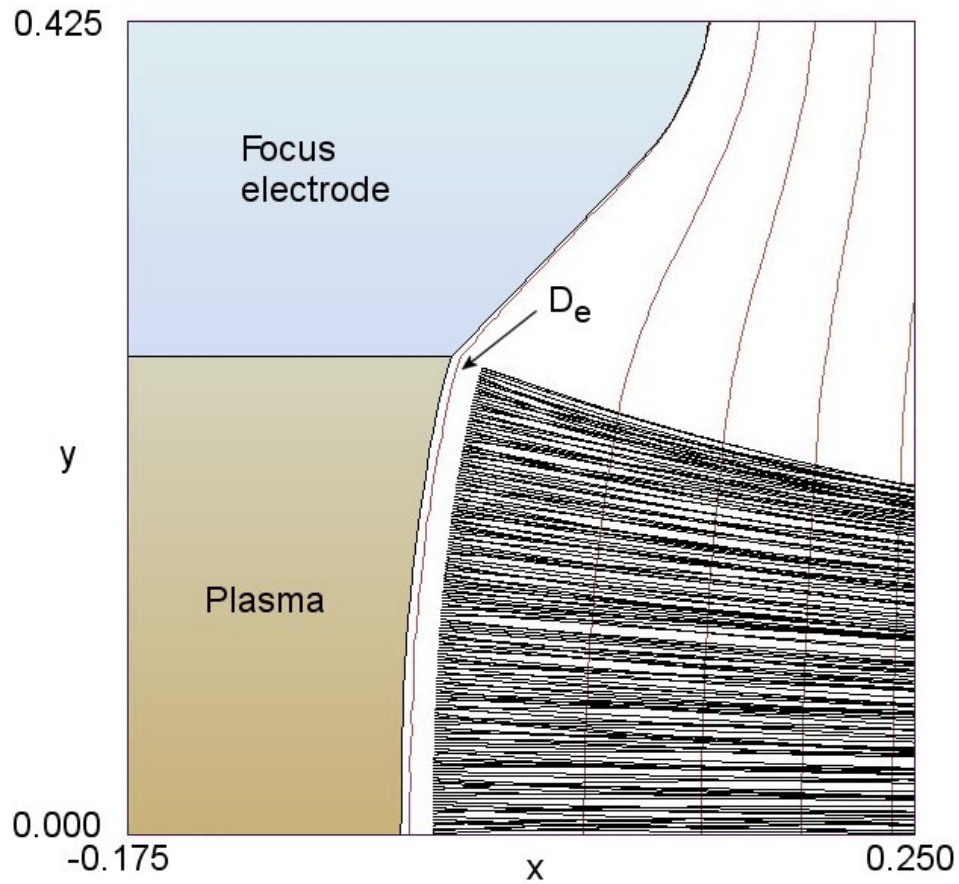


**Figure 10.** High-accuracy solution for the geometry of Fig. 8. Detailed view of the extraction region showing the calculated plasma surface, equipotential lines and particle orbits. Note that deuterons are launched with an angular divergence of  $15^\circ$ .